PCCP

Two-dimensional ^{67}Zn HYSCORE spectroscopy reveals that Zn-Bacteriochlorophyll a' is the primary donor (P_{840}) in the Type-1 reaction centers of Chloracidobacterium thermophilum

Journal:	*Physical Chemistry Chemical Physics*
Manuscript ID	CP-ART-12-2019-006556.R1
Article Type:	Paper
Date Submitted by the Author:	14-Feb-2020
Complete List of Authors:	Charles, Philip; Rensselaer Polytechnic Institute, Chemistry and Chemical Biology Kalendra, Vidmantas; Rensselaer Polytechnic Institute, Chemistry and Chemical Biology He, Zhihui; Pennsylvania State University, Biochemistry and Molecular Biology, 403 Althouse Laboratory Khatami, Mohammad; Brock University, Chemistry Golbeck, John; The Pennsylvania State University, Biochemistry and Molecular Biology van der Est, Art; Brock University, Chemistry Lakshmi, K. V.; Rensselaer Polytechnic Institute, Chemistry and Chemical Biology Bryant, Don; Pennsylvania State University, Biochemistry and Molecular Biology

PCCP

ARTICLE

Two-dimensional ^{67}Zn HYSCORE spectroscopy reveals that a Zn-Bacteriochlorophyll a_P' dimer is the primary donor (P_{840}) in the Type-1 reaction centers of *Chloracidobacterium thermophilum*

Received 00th January 20xx,
Accepted 00th January 20xx

DOI: 10.1039/x0xx00000x

Philip Charles,[a,‡] Vidmantas Kalendra,[a,‡] Zhihui He,[b,†] Mohammad Hassan Khatami,[d,†] John H. Golbeck,[b,c] Art van der Est,[d,*] K. V. Lakshmi[a,*] and Donald A. Bryant[b,e,*]

Chloracidobacterium (*C.*) *thermophilum* is a microaerophilic, chlorophototrophic species in the phylum *Acidobacteria* that uses homodimeric type-1 reaction centers (RC) to convert light energy into chemical energy using (bacterio)chlorophyll ((B)Chl) cofactors. Pigment analyses show that these RCs contain BChl a_P, Chl a_{PD}, and Zn^{2+}-BChl a_P' in the approximate ratio 7.1:5.4:1. However, the functional roles of these three different Chl species are not yet fully understood. It was recently demonstrated that Chl a_{PD} is the primary electron acceptor. Because Zn^{2+}-(B)Chl a_P' is present at low abundance, it was suggested that the primary electron donor might be a dimer of Zn^{2+}-BChl a_P' molecules. In this study, we utilize isotopic enrichment and high-resolution two-dimensional (2D) ^{14}N and ^{67}Zn hyperfine sublevel correlation (HYSCORE) spectroscopy to demonstrate that the primary donor cation, P_{840}^+, in the *C. thermophilum* RC is indeed a Zn^{2+}-BChl a_P' dimer. Density functional theory (DFT) calculations and the measured electron-nuclear hyperfine parameters of P_{840}^+ indicate that the electron spin density on P_{840}^+ is distributed nearly symmetrically over two Zn^{2+}-(B)Chl a_P' molecules as expected in a homodimeric RC. To our knowledge this is the only example of a photochemical RC in which the Chl molecules of the primary donor are metallated differently than those of the antenna.

Introduction

In chlorophototrophic organisms, light-induced electron transfer takes place in chlorophyll (Chl) containing membrane protein complexes called reaction centers (RCs) or photosystems. These complexes can be divided in two classes referred to as Type-1 or Type-2 depending on the nature of the terminal electron acceptors. However, in both types, the overall structure and arrangement of the cofactors are very similar with two branches of cofactors extending across the membrane from a Chl dimer called P_λ, where λ is the wavelength of its maximal absorbance bleaching. The first two cofactors of each branch are a so-called accessory chlorophyll and a chlorophyll or pheophytin. In Type-1 RCs, the electron transfer cofactors are also surrounded by a large number, ~60 to 90, antenna Chls. Excitation of the complex leads to energy transfer from the antenna Chls to the primary donor followed by electron transfer that results in charge separation between the dimer and the second Chl or pheophytin. In all known RCs, the dimer, the accessory Chl and the antenna Chl are all of the same type and contain the same metal.[1-3]

Hyperfine spectroscopy methods, such as, electron nuclear double resonance (ENDOR) and electron spin echo envelope modulation (ESEEM) have been widely used to study the structure and function of RCs[4-12] and other biological systems.[13-16] These methods probe the interactions of the unpaired electron spin(s) with proximal magnetic nuclei and provide information about the spin-density distribution, which is sensitive to the geometry and protein co-factor interactions. Most commonly, proton and nitrogen hyperfine couplings are measured but metals such as manganese have also been studied. However, the detection of magnetic couplings using ^{67}Zn hyperfine spectroscopy has been noticeably absent despite the importance of zinc in biological systems.

Recently, RCs from the moderately thermophilic, green bacterium *Chloracidobacterium* (*C.*) *thermophilum* have been characterized and shown to have an unusual composition.[17-20] *C.*

[a.] *Departments of Chemistry and Physics and The Baruch '60 Center for Biochemical Solar Energy Research, Rensselaer Polytechnic Institute, Troy, NY 12180, USA.*
[b.] *Department of Biochemistry and Molecular Biology, The Pennsylvania State University, State College, PA 16802, USA.*
[c.] *Department of Chemistry, The Pennsylvania State University, State College, PA 16802, USA.*
[d.] *Department of Chemistry, Brock University, St. Catharines, ON, Canada, L2S 3A1.*
[e.] *Department of Chemistry and Biochemistry, Montana State University, Bozeman, MT 59717, USA.*
** Corresponding authors.*
‡ These authors contributed equally to this work.

Electronic Supplementary Information (ESI) available: CW and HYSCORE spectra of Zn^{2+}-protoporphyrin IX and *C. thermophilum* membranes, electron charge density distribution in the P_{800}^+ and Zn^{2+}-protoporphyrin IX cation and hyperfine and quadrupolar parameters of the Zn^{2+}-protoporphyrin IX and dimeric Zn^{2+}-BChl g' cation. See DOI: 10.1039/x0xx00000x

thermophilum is an anoxygenic microaerophilic photoheterotroph, and like all other green bacteria, it employs chlorosomes as its major light-harvesting antenna.[19-22] To date, it is the only known chlorophototrophic member of the phylum *Acidobacteria*.[20] The other components of the photosynthetic apparatus in *C. thermophilum* most closely resemble those found in green sulfur bacteria. For example, unlike chlorosome-containing members of the *Chloroflexi* (e.g., *Chloroflexus aurantiacus* or *Oscillochloris trichoides*), the BChl a_P-binding Fenna-Matthews-Olson (FMO) protein is present.[23,24] Most interestingly, *C. thermophilum* possesses homodimeric Type-1 RCs that contain three different types of Chls: Mg-BChl a_P, Mg-Chl a_{PD}, and Zn-BChl a_P' in a ratio of *approx*. 7.1:5.4:1.[25] Moreover, the organism uses chlorosomes and FMO for light harvesting and it synthesizes (B)Chl *c* in addition to (B)Chl a_P, Chl a_{PD}, and Zn-(B)Chl a_P'. These findings were surprising as no other Type I RC in photosynthesis contains more than two types of (B)Chls and there are very few organisms that naturally produce Zn-BChl a_P.[26,27]

The highly unusual pigment composition of the *C. thermophilum* RC prompted us to characterize these complexes in greater detail to determine what roles the three different types of Chls play. Through studies with uniformly ^{15}N-labeled cells and membranes by photochemically induced dynamic nuclear polarization (photo-CIDNP), Zill et al. demonstrated that Chl a_{PD} is the primary electron acceptor in the RC.[28] The maximal light-induced bleaching occurs at 840 nm, which implies that the primary donor should either be Mg-BChl a_P or Zn-BChl a_P'.[22,25] The fact that Zn-BChl a_P' is present in a very low stochiometric ratio in the RC suggests that it might be the primary donor. However, Mg-BChl a_P and Zn-BChl a_P' cannot easily be distinguished from their optical properties. The possibility that the primary donor of the *C. thermophilum* RC may contain a different metal than the other Chls raises intriguing questions such as how the Zn-BChl a_P' would be bound selectively to the primary donor binding site and what influence the different metal would have on the primary photochemistry.

Although zinc plays a significant role in a number of fundamental biological processes and is found in a wide variety of proteins, in the absence of X-ray crystal structures the direct detection of Zn(II) bound to proteins is difficult because commonly used analytical methods, such as UV/vis and conventional electron paramagnetic resonance (EPR) spectroscopy, are not applicable.[29,30] Because ^{67}Zn is an isotope with a nuclear spin, I = 5/2, nuclear magnetic resonance (NMR) spectroscopy can provide information on the molecular structure and dynamics of the metal site. However, it has been challenging to detect ^{67}Zn using NMR due to the low gyromagnetic ratio ($\gamma = 1.6768 \times 10^7$ rad T^{-1} s^{-1}), low natural abundance (4.11%), inconvenient relaxation characteristics (e.g. very long longitudinal or very short transverse relaxation times), and extremely broad powder patterns arising from large anisotropic NMR interactions (e.g. moderately large nuclear quadrupole moment of 0.16×10^{28} Q/m^2).[31-33] Early studies by Oldfield and coworkers demonstrated the applicability of solid-state ^{67}Zn NMR in non-cubic zinc compounds[30] and more recently, Wu, Powers and others have reported natural abundance ^{67}Zn NMR of tetrahedral and octahedral Zn(II) complexes with O, N, S, Se and Te ligands.[29,31,34,35] These studies have been extended to the observation of ^{67}Zn in Zn(II)-containing enzymes.[36-40] However, to date there are only a limited number of solid-state ^{67}Zn NMR studies in literature,[33] and the applicability of ^{67}Zn NMR in paramagnetic charge-transfer intermediates of redox proteins is yet to be explored.

A method that is ideally suited to the detection of ^{67}Zn paramagnetic proteins is two-dimensional (2D) hyperfine sublevel correlation (HYSCORE) spectroscopy.[41] In HYSCORE spectroscopy, the magnetic nuclei that interact with the electron spin of a paramagnetic center are detected in two-dimensional frequency space, which dramatically improves the sensitivity of detection and spectral resolution. The nuclear frequencies are correlated in the two dimensions, which crucially simplifies analysis and can remove ambiguities in the interpretation of the experimental spectra. Most importantly, this allows for the observation broad signals that are hard to discern using one-dimensional hyperfine methods. These advantages render HYSCORE an optimal choice of method to test whether the primary donor cation of the *C. thermophilum* RC contains ^{67}Zn and to probe its hyperfine interactions. However, as mentioned earlier applications of ^{67}Zn hyperfine spectroscopy are lacking at this time.

In this study, we report ^{67}Zn-HYSCORE spectroscopic data on the oxidized primary donor, P_{840}^+, in *C. thermophilum* membranes containing RCs. Comparing uniformly ^{67}Zn labeled and unlabeled membranes containing RCs allows us to experimentally probe the role of ^{67}Zn-BChl a_P' in the primary photochemistry of *C. thermophilum*. In parallel, we also report density functional theory (DFT) calculations that predict the electron charge density distribution and electron-nuclear hyperfine and quadrupolar parameters of the primary donor cation, P_{840}^+, for comparison with the corresponding experimental data from the 2D HYSCORE measurements. Collectively, these studies clearly establish that the primary donor, P_{840}, in the *C. thermophilum* RC is a Zn-BChl a_P' dimer. This is the first evidence for the participation of Zn-BChl a_P' in the primary photochemistry of a photosynthetic RC. Furthermore, we believe this is also the first determination of the ^{67}Zn nuclear quadrupolar and hyperfine coupling constants in a paramagnetic intermediate of a protein and a related model system.

Methods

Medium preparation and growth of C. thermophilum cells: The *C. thermophilum* strain B^T was grown in CTM medium according to the procedures described in Tank and Bryant.[17,18] Slight changes in the medium were made to achieve growth of *C. thermophilum* on a medium containing ^{67}Zn. The $ZnSO_4$ in the CTM medium was replaced by 7 µM $^{67}ZnCl_2$, which was produced by dissolution of ^{67}Zn metal (Trace Sciences International Corp, Pilot Point, TX) in 12 N HCl. Cells were incubated at 53 °C in sealed bottles under microoxic conditions in an orbital shaking incubator (75 rpm) and were illuminated with a tungsten lamp at 50 µmol photons m^{-2} s^{-1} for 7 to 10 days prior to cell harvesting by centrifugation. Cells were stored at –80 °C until required.

Preparation of washed membranes and reaction centers from C. thermophilum: Washed membranes from *C. thermophilum* were purified by a method reported previously with some modifications.[28] *C. thermophilum* cells (from 5 L of culture; ~30 g wet weight) were harvested by centrifugation at 7,500 × *g* for 60 min. Cell pellets were resuspended in 60 ml of 50 mM 4-(2-hydroxyethyl)piperazine-1-ethanesulfonic acid (HEPES) buffer (pH 7.0) containing 1 mM phenylmethylsulfonyl fluoride, 2 mM dithiothreitol, and 3 mg of lysozyme ml^{-1}. The suspensions were incubated at room temperature in the dark for 30 min. The cell suspensions were kept on ice while the treated cells were disrupted by four passages through a chilled French pressure cell at

138 MPa. Unbroken cells and large cell debris were removed by centrifugation at 8,000 × *g* for 10 min, and the resulting supernatant was subjected to centrifugation at 220,000 × *g* for 1.5 h. The resulting pellet was resuspended in phosphate-buffered saline (PBS = 10 mM potassium phosphate pH 7.2, 150 mM NaCl) to an OD_{810} of 8 cm^{-1}. Chlorosome-depleted membranes were isolated on 10 to 50% (w/v) sucrose density gradients, which separated the greenish-brown, chlorosome-containing fraction from the orange-colored membranes that contained FMO and RCs.[25] The chlorosome-depleted membrane fraction was collected, diluted with the same buffer, and concentrated by ultrafiltration (50-kDa molecular mass cutoff; Millipore, Billerica, MA).

High performance liquid chromatography: The pigment composition of RC preparations was determined by RP-HPLC on an Agilent 1100 HPLC system (Agilent Technologies) equipped with an analytical Discovery C18 column (4.6 mm × 25 cm) (Supelco, Sigma-Aldrich) as described.[42] The gradient was composed of Solvent A (42% methanol, 33% acetonitrile, 25% water (v/v/v)) and Solvent B (50% methanol, 20% acetonitrile, 30% ethyl acetate (v/v/v)). At the time of injection, the mobile phase was 30% Solvent B at a flow rate of 1 ml min^{-1}. Solvent B was linearly increased to 100% over 50 min; this was followed by a constant flow of 100% Solvent B for 8 min after which Solvent B was returned to 30% in 2 min.

Isolation and validation of RCs from ^{67}Zn-labeled membranes: *C. thermophilum* RCs were purified from ^{67}Zn-labeled membranes and from unlabeled membranes as previously described,[22,25] and pigments were extracted with a mixture of acetone; methanol (7:2, vol/vol). The resulting pigment extract was subjected to preparative reversed-phase high-performance liquid chromatography (RP-HPLC) as previously described.[22,28] The peak corresponding to Zn-BChl a_P' was collected, concentrated, and subjected to mass spectrometric analysis as previously described.[22,25,28]

EPR spectroscopy: The EPR spectra were obtained on a custom-built continuous-wave (CW)/pulsed X-band Bruker Elexsys 580 EPR spectrometer using a dielectric flex-line ER 4118-MD5 probe (Bruker BioSpin, Billerica, MA) and a dynamic continuous-flow cryostat CF935 (Oxford Instruments, Oxfordshire, U.K.). The CW spectrum of *C. thermophilum* RC was acquired at 50 K under non-saturating conditions at an operating microwave frequency of 9.7 GHz, modulation frequency of 100 kHz, modulation amplitude of 0.3 mT and microwave power of 0.3 μW. The corresponding echo-detected magnetic-field-sweep EPR spectrum was measured at 20 K. The primary electron spin echo was generated using the pulse sequence ($\pi/2$–τ–π–τ–echo). The length of the $\pi/2$- and π-pulse was 8 ns and 16 ns, respectively, the inter-pulse separation, τ, was 108 ns and the delay in the pulse sequence is defined as the difference in the starting points of the pulses.

The 2D ^{14}N and ^{67}Zn HYSCORE spectra of the *C. thermophilum* RCs were acquired at 20 K and 5 K, respectively. The echo amplitude was measured using the pulse sequence ($\pi/2$–τ–$\pi/2$–t_1–π–t_2–$\pi/2$–τ–echo)[41] with a τ value of 156 ns and 136 ns for the ^{67}Zn and ^{14}N spectrum, respectively. The pulse length was 8 ns and 16 ns for the $\pi/2$- and π-pulses, respectively and the delays in the pulse sequence are defined as the difference in the starting point of the pulses. The echo intensity was measured as a function of t_1 and t_2, where t_1 and t_2 were incremented in steps of 16 ns from an initial value of 40 ns and 32 ns, respectively. 256 steps were used for each dimension. The 8 ns time difference between the initial value of t_1 and t_2 was set to account for the difference in length between the π/2- and π-pulse. This provided symmetric spectra in both dimensions. The unwanted echoes were eliminated by applying a 16-step phase cycling procedure.

The CW spectrum of the Zn-protoporphyrin IX cation was acquired at 50 K with an operating microwave frequency of 9.7 GHz, modulation frequency of 100 kHz, modulation amplitude of 3 G and microwave power of 0.2 μW. The corresponding echo-detected magnetic-field-sweep EPR spectrum and 2D ^{67}Zn HYSCORE spectrum of the Zn-protoporphyrin IX cation were acquired at 5 K. The echo amplitude was measured using the pulse sequence ($\pi/2$–τ–$\pi/2$–t_1–π–t_2–$\pi/2$–τ–echo) with a τ value of 136 ns and an 8 ns and 16 ns length for the $\pi/2$- and π-pulse, respectively. The time domain 2D HYSCORE data was processed using MATLAB R2018b. A third order polynomial baseline was subtracted from the resulting time-domain spectra. The corrected spectra were zero-filled to obtain [2048 x 2048] matrix and Fourier transformed using a Fast Fourier Transformation (FFT) algorithm. The frequency domain spectra were plotted as the amplitude (absolute value) of the 2D frequency components. The numerical simulations of the experimental 2D HYSCORE spectra using the hyperfine parameters obtained from the spectral analysis were performed with the "saffron" function of the EasySpin software package.[43]

Density functional theory: The DFT calculations of the BChl g_F' dimer and Zn^{2+}-BChl g_F' dimer were performed with a TPSSh functional and EPR-II/6-31G(d) basis set using the software program, ORCA 4.0.[44,45] The EPR-II basis set was used for the lighter atoms in the models while the 6-31G(d) basis set was incorporated for the Zn^{2+} ion. The RIJCOSX approximation was employed in conjunction with the CPCM solvent model with a dielectric (ε) of 4.0 to approximate the surrounding protein environment. The coordinates for the atoms in the computational model for the BChl g_F'dimer were derived from the X-ray coordinates of P_{800} of the RC from *Heliobacterium modesticaldum* (PDB ID: 5V8K).[3] The model for the Zn^{2+}-BChl g_F'dimer that was used to mimic the Zn^{2+}-BChl a_P' molecules that comprise the primary donor, P_{840}, in the *C. thermophilum* RC was constructed from the coordinates for the P_{800} primary donor (PDB ID: 5V8K) by replacing the central Mg^{2+} ion with Zn^{2+}. The structure was initially optimized using the software program, Avogadro[46] and subsequently refined in ORCA. Both dimeric models contained the complete BChl molecules with the exception that the isoprenoid substituent was replaced by a methyl group. Each model contained a total of 164 atoms. In order to estimate the effect of the exchange functional and basis set employed in the *ab initio* calculations, the electron spin density distribution, hyperfine and quadrupolar parameters that were obtained with the TPSSh functional and EPR-II/6-31G(d) basis set were compared with those obtained by using the same basis set with the BP, PBE0, and B3LYP functional. Similarly, the magnetic parameters were also calculated using either a B3LYP or TPSSh functional with a range of basis sets for the Zn atom, such as, 6-31G(d), 6-31G(f), def2-SVP and EPR-II. We observed that the TPSSh functional with the EPR-II/6-31G(d) basis provided the best match for the experimental hyperfine coupling constants. In general, the calculated hyperfine and quadrupolar parameters were validated by comparison with the analogous coupling constants that were determined by experimental 2D ^{14}N and ^{67}Zn HYSCORE spectroscopy and *vice versa*. Additionally, the computational methods were benchmarked by calculating the quadrupolar parameters of ^{67}Zn in the model compound, tetrakis(thiourea)zinc nitrate ($Zn^{2+}(thiourea)_4(NO_3)_2$).[47] The calculated quadrupolar coupling, C_Q, that was obtained with a TPSSh functional and EPR-II/6-31G(d) basis set was 3.52 MHz, which was 1.12 times larger

than the experimental value of 3.15 ± 0.05 MHz determined by Ida and Wu (2002). This was within the range of acceptable computed values in the study, where the authors had evaluated the accuracy of various computational methods for calculating ^{67}Zn quadrupolar parameters in molecular complexes. This indicates that the DFT methods used for estimating the quadrupolar couplings in the Zn^{2+}-BChl g_F′dimer were comparable with previous investigations.[47]

Results and Discussion

Continuous-wave EPR and 2D ^{14}N HYSCORE spectroscopy of the C. thermophilum membranes: Similar to the heterodimeric type-1 RC, PSI, of cyanobacteria and higher plants[1,48] and the homodimeric type-1 RC in heliobacteria (*Firmicutes*) and green sulfur bacteria (*Chlorobi*),[3] the electron-transfer pathway in the homodimeric type-1 RC in *C. thermophilum* is comprised of the primary donor, P_{840}, primary *Chl* a_{PD} electron acceptor, A_0, intermediate electron acceptor, A_{-1}, and three terminal [4Fe-4S] clusters, F_X, F_A and F_B.[19,22] In the present study, cryogenic illumination of the *C. thermophilum* membranes containing RCs at 77 K for 12 min leads to the photoaccumulation of a CW EPR signal at a *g*-value of 2.003 (Figure 1) due to the oxidized primary donor P_{840}^+. The peak-to-peak line width of the signal (0.8 mT) is narrower than the EPR signal of a monomeric BChl a_P cation *in vitro*. However, it is similar to the previously observed line widths of 0.7 mT, 1.0 mT and 1.3 mT for the primary donor cations, P_{700}^+, P_{798}^+ and P_{865}^+, of PSI, heliobacterial RCs and purple bacterial RC (bRC), respectively.[49-54] Previous studies have demonstrated that the narrower line widths of P_{700}^+ and P_{865}^+ arise from the wave function of the unpaired electron being distributed over both of the conjugated rings in the dimer. The close separation of 3-4 Å between the Chl a_P and Chl a_P′ heterodimer and BChl a_P dimer, respectively, allows strong electronic coupling between the (B)Chl rings, which leads to the delocalization.[49-54] Similarly, the narrow line width of the EPR signal in the present study suggests that the unpaired electron is also delocalized over the two Chls of the dimer in *C. thermophilum,* as expected in a homodimeric Type-1 RC.

Figures 2A and 2B show the respective experimental and simulated 2D ^{14}N HYSCORE spectra of P_{840}^+. The cross-peaks in the spectra arise from the hyperfine interactions of the unpaired electron spin (S = ½) with the nuclear spin (I = 1) of the nitrogen (^{14}N) atoms of P_{840}^+. The signals were acquired at a magnetic field position with maximum spectral intensity (345.8 mT) to ensure optimal signal to noise and resolution of the 2D HYSCORE spectrum. The spectrum contains cross-peaks that arise from four types of ^{14}N atoms, N^{I} – N^{IV}, that are hyperfine-coupled to the unpaired electron spin of P_{840}^+. Typically, the spectral features arising from ^{14}N atoms that are strongly hyperfine-coupled to the unpaired electron spin lead to cross-peaks in the (-,+) quadrant of a coupled ^{14}N atoms are observed in the (+,+) quadrant.[41] Thus, the pair of cross-peaks that are symmetric about the anti-diagonal in the (-,+) quadrant in Figure 2A are identified as double quantum

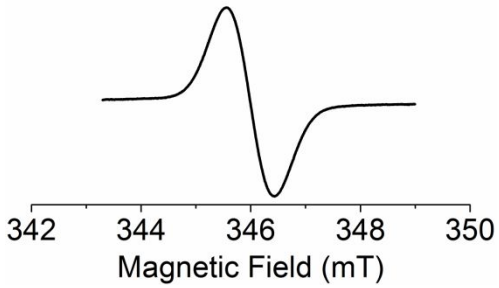

Figure 1. Continuous-wave EPR spectrum of the primary donor cation, P_{840}^+, of the *C. thermophilum* RC at 50 K. The spectrum displays a signal at g = 2.003 with a peak-to-peak line width of 0.8 mT.

(DQ) correlations of the ^{14}N atom, N^{I}, that is strongly hyperfine coupled (A > $2\nu_N$) to the unpaired electron spin of P_{840}^+. The separation between the cross-peaks is nearly four times the corresponding ^{14}N Zeeman frequency (ν_N = 1.07 MHz). In contrast, there are three closely spaced cross peaks in the (+,+) quadrant of the spectrum that are symmetric about the diagonal that are assigned to weakly hyperfine coupled ^{14}N atoms, N^{II} – N^{IV}. The first well-pronounced, intense cross peak in the (+,+) quadrant is located at a frequency ~1.31 MHz, which is close to the ^{14}N Zeeman frequency (1.07 MHz). This is assigned to the single quantum (SQ) transition of a weakly hyperfine-coupled (A < $2\nu_N$) ^{14}N atom, N^{II}. The small shift from the position corresponding to the ^{14}N Zeeman frequency is caused by the quadrupolar interaction of the nucleus. Additionally, there are two pairs of cross peaks of much weaker intensity that are also symmetric with respect to diagonal. These are assigned to the single- and double-quantum transition of the weakly coupled ^{14}N atoms, N^{III} and N^{IV}, respectively. Once again, the small shift along the diagonal from multiples of the Zeeman frequency is due to the nuclear quadrupolar interaction. The separation of all of the peaks along the diagonal is due to hyperfine interactions of the nucleus with the unpaired electron spin of P_{840}^+.

Knowledge of quadrupolar and hyperfine parameters is essential for the assignment of the ^{14}N atoms. The observation of pronounced DQ and SQ cross-peaks for N^{I} – N^{IV} permits determination of the hyperfine and quadrupolar parameters through numerical simulations. Each set of cross-peaks in the experimental spectrum is uniquely defined by the principal components of the hyperfine tensor, A_X – A_Z, in combination with the quadrupolar coupling constant and asymmetry parameter, K and η. The simulations provide an accurate determination of hyperfine components, A_X – A_Z, as well as the value of $K^2(3+\eta^2)$, where the quadrupolar coupling constant, $K = e^2qQ/4\hbar$, Q is the quadrupole moment interacting with the electric field gradient q, and η is the asymmetry parameter. The best fit of the simulated (Figure 2B) and experimental (Figure 2A) spectrum is obtained with the hyperfine and quadrupolar parameters that are presented in Table 1.

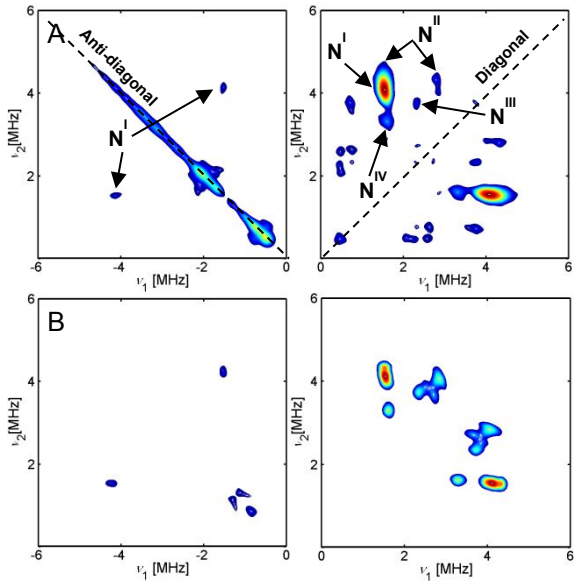

Figure 2. (A) Experimental and **(B)** simulated 2D ^{14}N HYSCORE spectrum of the primary donor cation, P_{840}^+, of the *C. thermophilum* RC. The cross-peaks in the (-,+) and (+,+) quadrant arise from the hyperfine interactions of the unpaired electron spin with four nitrogen-14 atoms (nuclear spin, I = 1), $N^I - N^{IV}$. The experimental spectrum was acquired at 20 K.

Nucleus	A_x (MHz)	A_y (MHz)	A_z (MHz)	A_{iso} (MHz)	K (MHz)	η
N^I	1.6 ± 0.2	0.5 ± 0.1	0.6 ± 0.1	0.90 ± 0.2	0.64 ± 0.04	0.6 ± 0.2
N^{II}	1.0 ± 0.2	1.8 ± 0.2	0.5 ± 0.1	1.10 ± 0.2	0.69 ± 0.04	0.8 ± 0.2
N^{III}	1.1 ± 0.2	1.0 ± 0.2	0.7 ± 0.2	0.90 ± 0.2	0.62 ± 0.05	0.3 ± 0.2
N^{IV}	1.0 ± 0.2	0.95 ± 0.2	1.05 ± 0.2	1.00 ± 0.2	0.32 ± 0.05	0.75 ± 0.2

Table 1. Experimental ^{14}N hyperfine (A) and quadrupolar (K) parameters of the primary donor cation, P_{840}^+, of the *C. thermophilum* RC that were obtained from the 2D HYSCORE spectroscopy measurements.

The value of the quadrupolar coupling constant, K, of 0.64 MHz for the strongly interacting nitrogen atom, N^I, is similar to the K value of 0.62 - 0.69 MHz of the weakly interaction nitrogens, N^{II} and N^{III} (Table 1). Based on previously published literature, N^I - N^{III}, are assigned to the nitrogen atoms in the BChl a_P′ ring(s) of the primary donor cation, P_{840}^+.[55-57] In contrast, the K value of 0.32 MHz for the nitrogen atom(s), N^{IV}, suggests that this is an imino nitrogen atom of histidine residue(s) that is/are likely axially coordinated to the central metal ion(s) of P_{840}^+.[6,58-62] The value of $e^2qQ/\hbar$ has been reported to be ~ 3.3 ± 0.3 MHz for an uncoordinated imino ^{14}N atom of an imidazole group. However, upon coordination with a transition metal ion this value is reduced to ~ 1.6 – 2.0 MHz, which corresponds to a value of 0.4 – 0.5 for K.[58,63-65] Thus, the observed quadrupolar constant, K, of 0.32 for N^{IV} is close to the range of values reported for the imino nitrogen of a histidine and is in agreement with previous observations that a histidine residue is axially coordinated to the central Mg(II) ion of the primary donor Chl a_P/Chl a_P′heterodimer and BChl a_P′dimer of PSI and bRC from purple bacteria, respectively.[1,2]

Interestingly, the value of the Fermi contact term or isotropic hyperfine interaction, A_{iso}, for all of the ^{14}N atoms, $N^I - N^{IV}$, of P_{840}^+ is between 0.9 – 1.0 MHz (Table 1). This is also reflected in the value of the three principal components, $A_X - A_Z$, of the hyperfine tensor. The A_{iso} value of the nitrogens, $N^I - N^{III}$, in the present study is smaller than was previously observed for a monomeric BChl a_P cation *in vitro*.[66-68] Moreover, it is in agreement with the values that were recorded for the primary donor cation of the bRC.[67] The smaller hyperfine coupling constants for the $N^I - N^{III}$ nitrogen atoms indicate that the unpaired electron spin is highly delocalized over the Mg-BChl a_P or Zn-BChl a_P′rings of P_{840}^+. This confirms that both the CW and pulsed EPR signals (Figures 1 and 2A-B) arise from the primary donor cation, P_{840}^+, of the *C. thermophilum* RC but do not identify which of the two BChls form the dimer.

^{67}Zn HYSCORE spectroscopy of the Zn^{2+}-protoporphyrin IX cation: If Zn(II) is the central metal ion in the BChl a_P′molecules of P_{840}^+, its hyperfine couplings should be detectable in HYSCORE measurements of ^{67}Zn-labeled samples. However, because there are no such measurements reported in the literature, we first assessed the feasibility of conducting 2D ^{67}Zn HYSCORE spectroscopy by studying the Zn^{2+}-protoporphyrin IX cation generated *in vitro* by cryogenic illumination.[69] Having confirmed the formation of the Zn^{2+}-protoporphyrin IX cation by CW EPR measurements at 50 K (Figure 1S), we acquired the 2D ^{67}Zn HYSCORE spectrum at 5 K. The premise is that, because ^{67}Zn is a heavier element than ^{14}N, it likely undergoes rapid transverse relaxation at 20 K. Hence, decreasing the temperature to 5 K would lead to a slower spin relaxation that could facilitate the spectroscopic detection of ^{67}Zn hyperfine interactions. Additionally, acquisition of the spectrum at 5 K would also enhance the Boltzmann factor and reduce the ambient noise in the HYSCORE experiment. A combination of these influences resulted in the successful observation of pronounced cross-peaks in the 2D ^{67}Zn-HYSCORE spectrum of the Zn^{2+}-protoporphyrin IX cation (Figure 2SA). However, the cross-peaks from the hyperfine coupled nitrogen atoms were not observed at 5 K because slower ^{14}N relaxation led to severe saturation of the signals. This is an advantage because temperature effects select for the ^{67}Zn cross-peaks and minimize interference from ^{14}N spectral features. The cross-peaks in the 2D ^{67}Zn-HYSCORE spectrum (Figure 2SA) that are symmetric about the main diagonal arise from the weak hyperfine couplings of ^{67}Zn (nuclear spin, I = 5/2) with the unpaired electron spin (S = ½) of the Zn^{2+}-protoporphyrin IX cation. Numerical simulations (Figure 2SB) of the experimental spectrum (Figure 2SA) yield isotropic hyperfine, A_{iso}, and quadrupolar parameters, K and η, for the ^{67}Zn atom that are presented in Table 1S. As far as we are aware, this represents the first example in which the presence of ^{67}Zn is detected in a paramagnetic environment by the application of pulsed hyperfine spectroscopy. Furthermore, observation of ^{67}Zn hyperfine couplings in the Zn^{2+}-protoporphyrin

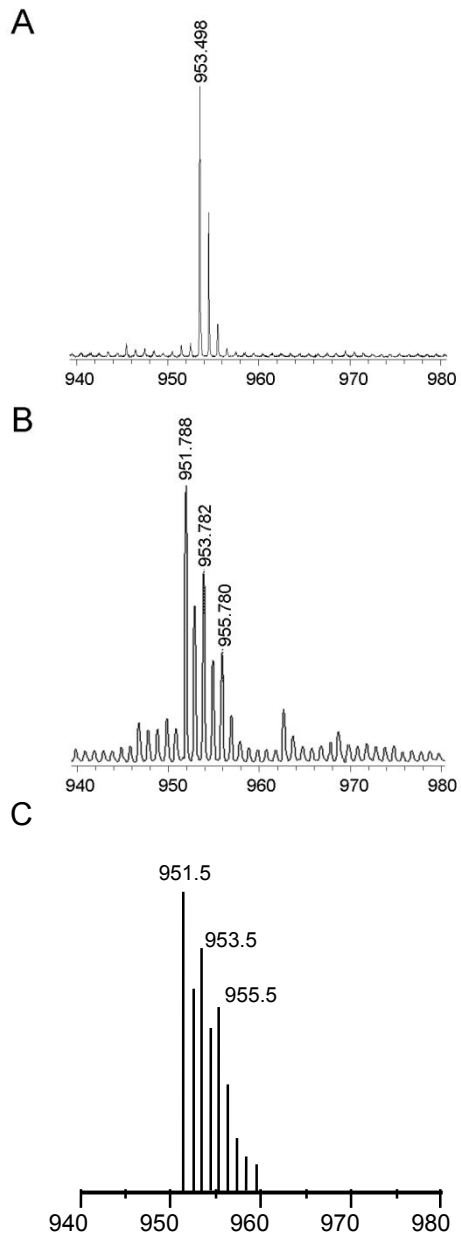

Figure 3. Mass spectroscopic analysis of Zn-BChl a_P'. Zn-BChl a_P' was isolated by HPLC as previously described from purified reaction centers prepared from cells grown in a medium containing ^{67}Zn **(A)** or with Zn of natural isotopic abundance **(B)** for Zn-BChl a_P' and subjected to mass spectroscopic analysis.[22,25,28] Panel **(C)** shows a simulated mass spectrum for natural abundance Zn-BChl a_P'. Note the simpler isotopic pattern in panel A, the principal M^+ ion at 953.498 for ^{67}Zn-BChl a_P', and in particular the absence of the lighter M^+ = 951.7 and 952.7 ions.

IX cation establishes the feasibility of conducting similar measurements on the *C. thermophilum* RC.

2D ^{67}Zn-HYSCORE spectroscopy of the ^{67}Zn-labeled C. thermophilum membranes: Based on the successful detection of ^{67}Zn in the Zn^{2+}-protoporphyrin IX cation, we conducted 2D ^{67}Zn-HYSCORE spectroscopy at 5 K to observe natural abundance ^{67}Zn hyperfine couplings in the primary donor cation, P_{840}^+, of *C. thermophilum* membranes containing RCs. These measurements did not yield any spectroscopic signals (Figure 3SB), likely due to (i) the low sensitivity (γ of 1.6768 □x 10^7 rad T^{-1} s^{-1}) and low isotopic abundance (4.11%) of ^{67}Zn; and (ii) relatively high molecular weight of the membranes; hence, there is a lower spin concentration for the *C. thermophilum* membranes containing RCs (in comparison with Zn^{2+}-protoporphyrin IX cation). This required us to isolate membranes from cells uniformly labeled with ^{67}Zn. We assessed the incorporation of the ^{67}Zn isotope by mass spectrometric analyses of Zn-BChl a_P' prepared from RCs isolated from membranes of *C. thermophilum* cells that had been uniformly labeled with ^{67}Zn. RCs were isolated as described by He et al. (2019),[25] Zn-BChl a' was then isolated from these RCs by preparative reversed-phase high-performance liquid chromatography (RP-HPLC),[22,28] and mass spectrometry was conducted on the peak corresponding to Zn-BChl a_P'.[25] These analyses showed that the mass ion for Zn-BChl a_P' from the labeled RCs was 953.5, as expected for the presence of ^{67}Zn-BChl a_P' (Figure 3). Masses (951.7 and 952.7) corresponding to lighter Zn isotopes were not detected in the Zn-BChl a_P' fraction from the labeled RCs. These results show that the RCs in membranes from cells uniformly labeled with ^{67}Zn exclusively contained ^{67}Zn-BChl a_P' as expected (Figure 3). A comprehensive characterization of other biochemical and biophysical properties of the *C. thermophilum* RCs is presented in He et al. (2019).[25]

We compared the 2D ^{67}Zn HYSCORE spectrum of natural abundance and ^{67}Zn-labeled *C. thermophilum* membranes containing RCs to estimate the sensitivity enhancement by isotopic enrichment (Figure 3SA-B). We observed that the 2D ^{67}Zn HYSCORE spectrum of P_{840}^+ in ^{67}Zn-labeled *C. thermophilum* membranes displayed a pair of cross-peaks (Figure 3SA and 4A) that were previously not visible in the analogous natural abundance membranes (Figure 3SB). This is consistent with the high (nearly 100%) isotopic enrichment of ^{67}Zn in the ^{67}Zn-labeled *C. thermophilum* membranes that was determined by mass spectrometry (Figure 3) and indicates that the primary donor cation, P_{840}^+, in the ^{67}Zn-labelled *C. thermophilum* membranes contains Zn-BChl a_P'. The two cross-peaks that are symmetric with respect to the main diagonal in the (+,+) quadrant of the spectrum (Figure 4A) arise from the hyperfine couplings of the central ^{67}Zn atom(s) (nuclear spin, I = 5/2) of the Zn-BChl a_P' dimer with the unpaired electron spin (S = ½) of P_{840}^+. The isotropic hyperfine coupling constant, A_{iso}, quadrupolar coupling constant, K, and asymmetry parameter, η, for the ^{67}Zn signals that were extracted from numerical simulations (Figure 4B) are shown in Table 2. In the simulations, we obtained a better fit of the experimental spectrum (Figure 4B) by using two ^{67}Zn sites, Zn^I and Zn^{II}, with slightly different hyperfine coupling parameters. This suggests that it is possible to distinguish dissimilar ^{67}Zn sites by the application of 2D ^{67}Zn HYSCORE spectroscopy.

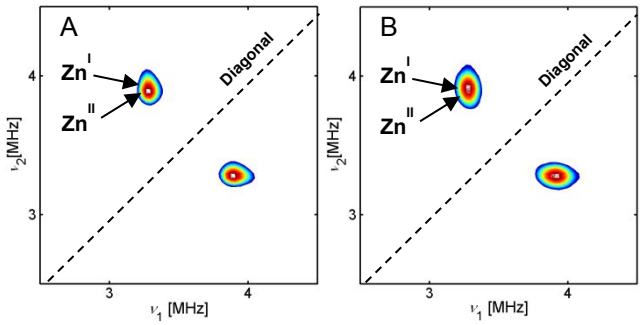

Figure 4. (A) Experimental and **(B)** simulated 2D ^{67}Zn HYSCORE spectrum of the primary donor cation, P_{840}^+, of the ^{67}Zn-labeled *C. thermophilum* RC in membranes. The cross-peaks in the spectrum are attributed to the hyperfine interactions of the unpaired electron spin with the ^{67}Zn atom(s) (nuclear spin, I = 5/2). The experimental spectrum was acquired at 5 K which favors observation of the magnetic interactions with ^{67}Zn due to rapid spin relaxation.

Nucleus	A_x (MHz)	A_y (MHz)	A_z (MHz)	A_{iso} (MHz)	K (MHz)	η
Zn^I	0.28 ± 0.03	0.84 ± 0.05	0.71 ± 0.04	0.61 ± 0.04	0.80 ± 0.03	0.28 ± 0.11
Zn^{II}	0.27 ± 0.03	0.79 ± 0.05	0.71 ± 0.04	0.59 ± 0.04	0.80 ± 0.03	0.28 ± 0.11

Table 2. Experimental ^{67}Zn hyperfine (A) and quadrupolar (K) parameters of the primary donor cation, P_{840}^+, of the *C. thermophilum* RC that were obtained from the 2D HYSCORE spectroscopy measurements.

The location of the cross-peaks in the 2D ^{67}Zn HYSCORE spectrum of P_{840}^+ (Figure 4A) depends on the quadrupolar coupling constant and asymmetry parameter, K (also referred to as ν_Q in literature) and η, respectively, and hyperfine coupling constant, A. It is known that K and η arise from the interplay of the nuclear quadrupolar moment (Q) with the local electric field gradient (q) at the nucleus. The quadrupolar interaction is proportional to the inverse cube of the separation ($1/r^3$) between the nucleus of interest and charge density contributing to the electric field gradient. Therefore, it reflects the local structure and symmetry at the nucleus, where K provides insight on the local "spherical" symmetry and η reflects the "axial" symmetry of the local ground-state electronic environment. As a result, the presence of higher asymmetry in the coordination environment of the ^{67}Zn site results in larger quadrupolar coupling constants. For example, octahedral complexes yield quadrupolar constants, C_Q, in the range of 2.6 - 4.0 MHz, while in tetrahedral complexes the values of C_Q are significantly larger (~14 - 15 MHz) (where C_Q is defined as K(2I(2I-1))).[70] The larger values of C_Q reflect the relative distortion around the Zn(II) ion upon decreasing the coordination number in the tetrahedral complexes relative to octahedral ones. Additionally, previous solid-state NMR studies have demonstrated that the quadrupolar parameters are also sensitive to the nature of the bound ligands[39], indicating that ^{67}Zn is sensitive to changes in both the structure and bonding of a specific site.

In the 2D ^{67}Zn HYSCORE spectrum of P_{840}^+, the first-order quadrupolar interactions result in frequency shifts of the cross-peaks parallel to the diagonal. The size of the shift depends on the quadrupolar coupling constant, K. The hyperfine coupling, A, affects the separation between the pair of cross peaks. In comparison, the effects of the second-order quadrupolar interactions are much smaller. Of course, one of the questions is how the ^{67}Zn quadrupolar and hyperfine tensor in this study relate to the chemical environment and molecular structure of the zinc-binding site. The quadrupolar coupling parameters, K and η, of 0.8 MHz (C_Q = 16 MHz) and 0.28, respectively, that are obtained from the spectral simulations of the 2D ^{67}Zn HYSCORE spectrum (Table 2) indicate that the zinc coordination environment in the primary donor BChl a_P' dimer of P_{840}^+ is moderately asymmetric. The observed C_Q value of 16 MHz is slightly larger than previously reported for tetrahedral complexes, such as, $[Bp]_2Zn$ (C_Q of 13.66 MHz), while it is much larger than $Zn(ClO_4)_2{\cdot}6H_2O$ (C_Q of 0.2 MHz) and ZnSe (negligible C_Q) that contain an octahedral Zn site with nearly perfect symmetry.[31] The C_Q value of ^{67}Zn in zinc metal has been reported to be 11.98 MHz[71,72] but it is not reasonable to compare this value with the constants obtained for zinc coordination complexes.[31]

The common ligands in zinc enzymes are His (N), Asp (O), Glu (O), Cys (S), and H_2O/OH (O), where the C_Q values span a range of 38.75 MHz.[35] In the present study, the moderate value of C_Q and η of 16 MHz and 0.28, respectively, suggest square pyramidal ligand geometry around the ^{67}Zn atom as expected for an axially coordinated chlorin. The isotropic hyperfine coupling constant or Fermi contact term, A_{iso}, suggests the presence of distributed electron spin density on the ^{67}Zn atom in P_{840}^+. However, it is important to note that hyperfine coupling can occur as a result of polarization of the electrons in filled orbitals so that the orbital carrying the unpaired electron is not necessarily localized on the Zn atom. Because of this, the A_{iso} value of ~ 0.6 MHz that is observed for the Zn^I and Zn^{II} sites in P_{840}^+ is relatively small. Additionally, because the orbital is not localized on the metal, it is not expected that the A_{iso} value for ^{67}Zn that is observed in P_{840}^+ (Table 2) would be 50% of the A_{iso} value for the monomeric Zn^{2+}-protoporphyrin IX cation (Table 1S).

Density functional theory calculations of the primary donor cation of C. thermophilum: We performed DFT calculations to understand better the effects of the electronic structure and local symmetry on the hyperfine and quadrupolar parameters of the ^{67}Zn site(s) in the primary donor cation, P_{840}^+, of the *C. thermophilum* RC. The theoretical calculations complement the 2D ^{67}Zn HYSCORE measurements, and the experimental hyperfine and quadrupolar coupling parameters in turn validate the results of the *ab initio* calculations. To our best knowledge, quantum-mechanical calculations to determine the quadrupolar parameters of ^{67}Zn have only been conducted for Zn^{2+}-containing diamagnetic model complexes and active sites in proteins.[35,38,47,73]

In the absence of an X-ray crystal structure for the *C. thermophilum* RC, the computational models for P_{840}^+ that were used in the DFT calculations were derived from the structure of the

heliobacterial RC (HbRC).[3] We selected the HbRC as a starting point because it is a type-1 RC that is comprised of a homodimeric subunit core ($PshA_2$) that is similar to that the *C. thermophilum* RC.[20,25] Here, the presence of the surrounding homodimeric protein environment is important, as it has been demonstrated to have a profound effect on the distribution of the electron spin density in the primary donor cation, P_{800}^+, and similar effects are expected for P_{840}^+ of the *C. thermophilum* RC. Additionally, the DFT calculations on the P_{800}^+ cation of the HbRC served as a test case to reproduce the electron spin delocalization over the BChl g_F' dimer. Because the HYSCORE data discussed above indicate that P_{840}^+ is a Zn-containing BChl a_P' dimer, we replaced the Mg(II) in the HbRC model with Zn(II). The Chl in the HbRC model is BChl g_F', while P_{840}^+ in the *C. thermophilum* RC contains BChl a_P'. Hence, we attempted to build a Zn-BChl a_P' dimer model based on the HbRC structure. However, geometry optimization of this model resulted in an asymmetric structure, which is not reasonable in a homodimeric RC and not in agreement with the observed linewidths and hyperfine couplings. Thus, we have optimized the structure of the Zn^{2+}-BChl g_F' dimer to construct a computational model for P_{840}^+ (Figure 5). In the absence of any experimental structural data for P_{840}^+, it is difficult to estimate accurately how large the effect of using BChl g_F' instead of BChl a_P' would be. Nonetheless, we believe it should be relatively minor for the magnetic parameters of the central Zn(II) ion because the differences between the two types of chlorophyll occur at the periphery of the chlorin ring.

Previous computational studies of Zn(II)-containing proteins have used quantum mechanics/molecular modeling (QM/MM), which involves intensive quantum mechanical calculations on a small group of selected atoms, while Newtonian forces are used for the rest of the system. However, it has previously been reported that the predicted electric field gradient for ^{67}Zn is sensitive to the choice of the quantum region in such calculations.[74] Additionally, the strong electronic coupling between the BChl rings in the primary donor models, P_{800}^+ and P_{840}^+, would likely complicate the use of hybrid methods. Hence, we used an all-quantum mechanical approach to model the electronic structure of the cofactors as a whole. The DFT calculations indicated that a TPSSh functional employing an EPR-II/6-31G(d) basis set resulted in closest agreement with the experiment. Here, the EPR-II basis set was used for the lighter atoms in the computational model while the 6-31G(d) basis set was incorporated for the Zn atoms. The calculations of the P_{840}^+ model using a Zn^{2+}-BChl g_F' dimer corroborated the experimental hyperfine and quadrupolar parameters that were determined from the 2D HYSCORE measurements. As can be seen in Table 3S, the calculated isotropic hyperfine coupling constants for the Zn^I and Zn^{II} sites in the P_{840}^+ model are in excellent agreement with the experimentally determined values of ~ 0.6 MHz (Table 2). However, the DFT calculations overestimated the quadrupolar coupling constant, K, in comparison with the experimentally determined values. A similar trend was also observed in the experimental (Table 1S) and calculated (Table 2S) ^{67}Zn quadrupolar coupling constants of the Zn^{2+}-protoporphyrin IX cation, for which the calculated K value was slightly larger than the experimental coupling. There could be several reasons for this discrepancy. Similar to previous reports, our experience has been that the value of K calculated by DFT is sensitive to the basis set that is used to describe the Zn orbitals.[47] It is also possible that the difference in the K values in the present study could arise from the effect of using a BChl g_F' dimer in the P_{840}^+ computational model (instead of a BChl g_F' dimer) or due to the effects of excluding the electronic/electrostatic effects of the second coordination sphere residues on the ^{67}Zn site.[74] However, it has been reported that it is often sufficient to consider only ligands from the first coordination sphere around the zinc atom unless the Zn site is bound to water molecules that are involved in extensive hydrogen-bonding interactions.[47]

Based on a systematic evaluation of ^{67}Zn quadrupolar coupling constants that were obtained from restricted Hartree-Fock (RHF) and DFT-level calculations, the best calculated results for the ^{67}Zn quadrupolar tensor components in molecular coordination complexes have been shown to exhibit a standard error of 0.03 au, where 1 au corresponds to 35.244 MHz for ^{67}Zn.[47] We find that the errors encountered in the present study are within this range. The DFT calculations in the present study provide a reasonable estimate of the magnitude of hyperfine and quadrupolar parameters for the ^{67}Zn site of P_{840}^+. Moreover, the computational methods compare well with those used in previous studies that have included calculations on Zn(II) coordination complexes that exhibit very different quadrupolar coupling constants in a variety of coordination environments, including both tetrahedral and octahedral coordination arrangements and common ligand atoms, such as, O, N, and S.[47] Similar to current observations, previous

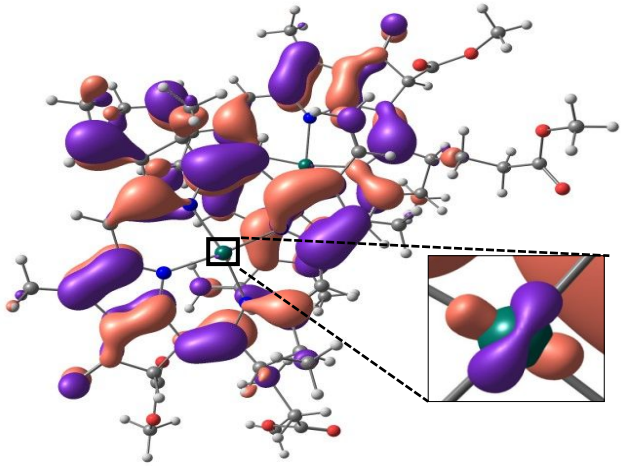

Figure 5. Electron charge density distribution in the singly occupied molecular orbital of the dimeric Zn^{2+}-BChl g_F' cation. The computational model was derived from the coordinates of the primary donor Mg^{2+}-BChl g_F' dimer from the X-ray crystal structure the heliobacterial reaction center[3] where the Mg^{2+} ions were replaced by Zn^{2+}. The electron charge density in the singly occupied molecular orbital is delocalized on both of the Zn^{2+}-BChl g_F' rings which is consistent with the narrower line width of the CW EPR spectrum and smaller ^{14}N hyperfine coupling constants that were observed for P_{840}^+.

studies have shown that for a given basis set, the calculations at the B3LYP level or higher yield consistently better agreement with the experimental data.[47] Additionally, the quality of the computed ^{67}Zn electric field gradient depended primarily on the quality of the basis set (e.g. medium basis set of 6-31G(f)) for the Zn atom was well suited).[47]

Conclusions

The 2D ^{67}Zn HYSCORE spectroscopy measurements provide direct evidence that the excitonically coupled BChl dimer in the primary donor cation, P_{840}^+, is comprised of Zn-BChl a_P' molecules. Supporting this conclusion, (1) the maximal light-induced bleaching at 840 nm,[22,25] (2) the relatively narrow line width of the *CW* EPR signal of P_{840}^+, (3) the smaller ^{14}N hyperfine coupling constants of the ring nitrogen atoms in comparison with monomeric Chl$^+$ and (4) DFT caculations showing a distributed electron density in a dimeric Zn^{2+}-BChl g_F' cation model all indicate that the charge density should be highly delocalized over a strongly excitonically coupled BChl dimer in the primary donor cation, P_{840}^+, of *C. thermophilum*. This is the first example of a photochemical RC in which the (B)Chl molecules in the primary donor are metallated differently than the other (B)Chls in the RC and antenna. In other respects, these unusual *C. thermophilum* RCs are nevertheless similar to other homodimeric type-1 RCs,[25] as the spin density in P_{840}^+ is distributed symmetrically over the two Chls of the dimer. This work also demonstrates the utility of 2D ^{67}Zn HYSCORE spectroscopy for the study of zinc sites in paramagnetic systems. By the direct detection of ^{67}Zn hyperfine and quadrupolar couplings in a paramagnetic excited state of a ^{67}Zn-labelled reaction center, we anticipate that in the future 2D ^{67}Zn HYSCORE spectroscopy will play an important role in the study of ^{67}Zn-enriched metalloproteins. Furthermore, a combination of 2D ^{67}Zn HYSCORE data and DFT calculations has the potential to be used as a tool to characterize Zn-containing paramagnetic systems with low ^{67}Zn concentrations. Overall, this study is a noteworthy contribution toward probing the relationship between ^{67}Zn hyperfine and quadrupolar interaction tensors and molecular structure in a paramagnetic system and provides excellent opportunities for the application of 2D ^{67}Zn HYSCORE in the investigation of zinc binding sites in a wide variety of bioinorganic systems.

Acknowledgements

This study is supported by the Photosynthetic Systems Program, Office of Basic Energy Sciences of the U. S. Department of Energy under the contract DE-FG02-07ER15903 (KVL), DE-FG02-94ER20137 (DAB) and DE-SC0010575 (JHG) and an NSERC Discovery grant RGPIN-2015-04021 (AvdE). The authors would like to acknowledge the Center for Computational Innovations (CCI) at Rensselaer Polytechnic Institute for computational resources.

Conflicts of interest

There are no conflicts to declare.

Notes and References

†Present Addresses

Zhihui He, Ph.D.
Washington University School of Medicine
Department of Cell Biology and Physiology
425 South Euclid Avenue
9th Floor BJCIH Room 9401
Saint Louis, MO 63110

Mohammad Hassan Khatami
University of Ontario Institute of Technology
Faculty of Science
Oshawa, Ontario L1H 7K4
Canada

(1) Jordan, P.; Fromme, P.; Witt, H. T.; Klukas, O.; Saenger, W.; Krauss, N. *Nature* **2001**, *411*, 909.
(2) Yeates, T. O.; Komiya, H.; Chirino, A.; Rees, D. C.; Allen, J. P.; Feher, G. *Proc. Natl. Acad. Sci. U. S. A.* **1988**, *85*, 7993.
(3) Gisriel, C.; Sarrou, I.; Ferlez, B.; Golbeck, J. H.; Redding, K. E.; Fromme, R. *Science* **2017**, *357*, 1021.
(4) Mac, M.; Tang, X. S.; Diner, B. A.; McCracken, J.; Babcock, G. T. *Biochemistry* **1996**, *35*, 13288.
(5) Mac, M.; Bowlby, N. R.; Babcock, G. T.; McCracken, J. *J. Amer. Chem. Soc.* **1998**, *120*, 13215.
(6) Deligiannakis, Y.; Hanley, J.; Rutherford, A. W. *J. Am. Chem. Soc.* **1999**, *121*, 7653.
(7) Deligiannakis, Y.; Rutherford, A. W. *Biochim. Biophys. Acta- Bioenergetics* **2001**, *1507*, 226.
(8) Lubitz, W.; Lendzian, F.; Bittl, R. *Acc. Chem. Res.* **2002**, *35*, 313.
(9) Britt, R. D.; Campbell, K. A.; Peloquin, J. M.; Gilchrist, M. L.; Aznar, C. P.; Dicus, M. M.; Robblee, J.; Messinger, J. *Biochim. Biophys. Acta- Bioenergetics* **2004**, *1655*, 158.
(10) Srinivasan, N.; Santabarbara, S.; Rappaport, F.; Carbonera, D.; Redding, K.; van der Est, A.; Golbeck, J. H. *J. Phys. Chem. B* **2011**, *115*, 1751.
(11) Srinivasan, N.; Chatterjee, R.; Milikisiyants, S.; Golbeck, J. H.; Lakshmi, K. V. *Biochemistry* **2011**, *50*, 3495.
(12) Taguchi, A. T.; O' Malley, P. J.; Wraight, C. A.; Dikanov, S. A. *J. Phys. Chem. B* **2017**, *121*, 10256.
(13) Prisner, T.; Rohrer, M.; MacMillan, F. *Annu. Rev. Phys. Chem.* **2001**, *52*, 279.
(14) Lyubenova, S.; Maly, T.; Zwicker, K.; Brandt, U.; Ludwig, B.; Prisner, T. *Acc. Chem. Res.* **2010**, *43*, 181.
(15) Lakshmi, K. V.; Brudvig, G. W. *Curr. Opin. Struct. Biol.* **2001**, *11*, 523.
(16) Deligiannakis, Y.; Louloudi, M.; Hadjiliadis, N. *Coord. Chem. Rev.* **2000**, *204*, 1.
(17) Tank, M.; Bryant, D. A. *Int. J Syst Evol. Microbiol.* **2015**, *65*, 1426.
(18) Tank, M.; Bryant, D. A. *Front. Microbiol.* **2015**, *6*, 226.
(19) Bryant, D. A.; Costas, A. M. G.; Maresca, J. A.; Chew, A. G. M.; Klatt, C. G.; Bateson, M. M.; Tallon, L. J.; Hostetler, J.;

Nelson, W. C.; Heidelberg, J. F.; Ward, D. M. *Science* **2007**, *317*, 523.

(20) Thiel, V.; Tank, M.; Bryant, D. A. In *Annu. Rev. Plant Biol., Vol. 69*; Merchant, S. S., Ed.; Annual Reviews: Palo Alto, 2018; Vol. 69, p 21.

(21) Costas, A. M. G.; Tsukatani, Y.; Romberger, S. P.; Oostergetel, G. T.; Boekema, E. J.; Golbeck, J. H.; Bryant, D. A. *J. Bacteriol.* **2011**, *193*, 6701.

(22) Tsukatani, Y.; Romberger, S. P.; Golbeck, J. H.; Bryant, D. A. *J. Biol. Chem.* **2012**, *287*, 5720.

(23) Tsukatani, Y.; Wen, J. Z.; Blankenship, R. E.; Bryant, D. A. *Photosynth. Res.* **2010**, *104*, 201.

(24) Wen, J. Z.; Tsukatani, Y.; Cui, W. D.; Zhang, H.; Gross, M. L.; Bryant, D. A.; Blankenship, R. E. *Biochim. Biophys. Acta-Bioenerg.* **2011**, *1807*, 157.

(25) He, Z.; Ferlez, B.; Kurashov, V.; Tank, M.; Golbeck, J. H.; Bryant, D. A. *Photosyn. Res.* **2019**, *142*, 87.

(26) Wakao, N.; Yokoi, N.; Isoyama, N.; Hiraishi, A.; Shimada, K.; Kobayashi, M.; Kise, H.; Iwaki, M.; Itoh, S.; Takaichi, S.; Sakurai, Y. *Plant Cell Physiol.* **1996**, *37*, 889.

(27) Tomi, T.; Shibata, Y.; Ikeda, Y.; Taniguchi, S.; Haik, C.; Mataga, N.; Shimada, K.; Itoh, S. *Biochim. Biophys. Acta-Bioenerg.* **2007**, *1767*, 22.

(28) Zill, J. C.; He, Z.; Tank, M.; Ferlez, B. H.; Canniffe, D. P.; Lahav, Y.; Bellstedt, P.; Alia, A.; Schapiro, I.; Golbeck, J. H.; Bryant, D. A.; Matysik, J. *Photosynth. Res.* **2018**, *137*, 295.

(29) Larsen, F. H.; Lipton, A. S.; Jakobsen, H. J.; Nielsen, N. C.; Ellis, P. D. *J. Am. Chem. Soc.* **1999**, *121*, 3783.

(30) Zhang, Y.; Mukherjee, S.; Oldfield, E. *J. Am. Chem. Soc.* **2005**, *127*, 2370.

(31) Sham, S.; Wu, G. *Can. J. Chem.-Rev. Can. Chim.* **1999**, *77*, 1782.

(32) Sutrisno, A.; Liu, L.; Xu, J.; Huang, Y. N. *Phys. Chem. Chem. Phys.* **2011**, *13*, 16606.

(33) Schurko, R. W. *Acc. Chem. Res.* **2013**, *46*, 1985.

(34) Wu, G. *Chem. Phys. Lett.* **1998**, *298*, 375.

(35) Mroue, K. H.; Power, W. P. *J. Phys. Chem. A* **2010**, *114*, 324.

(36) Wu, G. *Biochem. Cell Biol.* **1998**, *76*, 429.

(37) Lipton, A. S.; Buchko, G. W.; Sears, J. A.; Kennedy, M. A.; Ellis, P. D. *J. Am. Chem. Soc.* **2001**, *123*, 992.

(38) Lipton, A. S.; Bergquist, C.; Parkin, G.; Ellis, P. D. *J. Am. Chem. Soc.* **2003**, *125*, 3768.

(39) Lipton, A. S.; Heck, R. W.; Ellis, P. D. *J. Am. Chem. Soc.* **2004**, *126*, 4735.

(40) Ellis, P. D.; Lipton, A. S. In *Annu. Rep. NMR Spect., Vol. 60*; Webb, G. A., Ed.; Elsevier Academic Press Inc: San Diego, 2007; Vol. 60, p 1.

(41) Hofer, P.; Grupp, A.; Nebenfuhr, H.; Mehring, M. *Chem. Phys. Lett.* **1986**, *132*, 279.

(42) Frigaard, N.-U.; Takaichi, S.; Hirota, M.; Shimada, K.; Matsuura, K. *Arch. Microbiol.* **1997**, *167*, 343.

(43) Stoll, S.; Schweiger, A. *J. Magn. Reson.* **2006**, *178*, 42.

(44) Neese, F. *Wiley Interdiscip. Rev.-Comput. Mol. Sci.* **2012**, *2*, 73.

(45) Neese, F. *Wiley Interdiscip. Rev.-Comput. Mol. Sci.* **2018**, *8*, e1327.

(46) Hanwell, M. D.; Curtis, D. E.; Lonie, D. C.; Vandermeersch, T.; Zurek, E.; Hutchison, G. R. *J. Cheminformatics* **2012**, *4*, 17.

(47) Ida, R.; Wu, G. *J. Phys. Chem. A* **2002**, *106*, 11234.

(48) Grotjohann, I.; Fromme, P. *Photosynth. Res.* **2005**, *85*, 51.

(49) Norris, J. R.; Uphaus, R. A.; Crespi, H. L.; Katz, J. *Proc. Natl. Acad. Sci. U. S. A.* **1971**, *68*, 625.

(50) McElroy, J. D.; Mauzerall, D. C.; Feher, G. *Biochim. Biophys. Acta* **1972**, *267*, 363.

(51) Norris, J. R.; Scheer, H.; Katz, J. J. *Ann. New York Acad. Sci.* **1975**, *244*, 260.

(52) Feher, G.; Hoff, A. J.; Isaacson, R. A.; Ackerson, L. C. *Ann. New York Acad. Sci.* **1975**, *244*, 239.

(53) Lendzian, F.; Huber, M.; Isaacson, R. A.; Endeward, B.; Plato, M.; Bonigk, B.; Mobius, K.; Lubitz, W.; Feher, G. *Biochim. Biophys. Acta* **1993**, *1183*, 139.

(54) Allen, J. P.; Cordova, J. M.; Jolley, C. C.; Murray, T. A.; Schneider, J. W.; Woodbury, N. W.; Williams, J. C.; Niklas, J.; Klihm, G.; Reus, M.; Lubitz, W. *Photosynth. Res.* **2009**, *99*, 1.

(55) Garcia-Rubio, I.; Martinez, J. I.; Picorel, R.; Yruela, I. L.; Alonso, P. J. *J. Am. Chem. Soc.* **2003**, *125*, 15846.

(56) Deligiannakis, Y.; Louloudi, M.; Hadjiliadis, N. *Coord. Chem. Rev.* **2000**, *204*, 1.

(57) Van Doorslaer, S. *J. Magn. Reson.* **2017**, *280*, 79.

(58) Edmonds, D. T. *Phys. Rep.-Phys. Lett.* **1977**, *29*, 233.

(59) Milikisiyants, S.; Chatterjee, R.; Weyers, A.; Meenaghan, A.; Coates, C.; Lakshmi, K. V. *J. Phys. Chem. B* **2010**, *114*, 10905.

(60) Chatterjee, R.; Milikisiyants, S.; Coates, C. S.; Lakshmi, K. V. *Biochemistry* **2011**, *50*, 491.

(61) Coates, C. S.; Milikisiyants, S.; Chatterjee, R.; Whittaker, M. M.; Whittaker, J. W.; Lakshmi, K. V. *J. Phys. Chem. B* **2015**, *119*, 4905.

(62) Stich, T. A.; Yeagle, G. J.; Service, R. J.; Debus, R. J.; Britt, R. D. *Biochemistry* **2011**, *50*, 7390.

(63) Ashby, C. I. H.; Cheng, C. P.; Brown, T. L. *J. Am. Chem. Soc.* **1978**, *100*, 6057.

(64) Ashby, C. I. H.; Paton, W. F.; Brown, T. L. *J. Am. Chem. Soc.* **1980**, *102*, 2990.

(65) Astashkin, A. V.; Dikanov, S. A.; Tsvetkov, Y. D. *J. Struct. Chem.* **1984**, *25*, 45.

(66) Kass, H.; Rautter, J.; Zweygart, W.; Struck, A.; Scheer, H.; Lubitz, W. *J. Phys. Chem.* **1994**, *98*, 354.

(67) Kass, H.; Rautter, J.; Bonigk, B.; Hofer, P.; Lubitz, W. *J. Phys. Chem.* **1995**, *99*, 436.

(68) Lubitz, W.; Lendzian, F.; Plato, M.; Scheer, H.; Mobius, K. *Appl. Magn. Reson.* **1997**, *13*, 531.

(69) Gasyna, Z.; Browett, W. R.; Stillman, M. J. *Inorg. Chim. Acta-Bioinorg. Chem.* **1984**, *92*, 37.

(70) Lipton, A. S.; Wright, T. A.; Bowman, M. K.; Reger, D. L.; Ellis, P. D. *J. Am. Chem. Soc.* **2002**, *124*, 5850.

(71) Herberg, H.; Abart, J.; Voitlander, J. *Z. Naturfors. Sect. A-J. Phys. Sci.* **1979**, *34*, 1029.

(72) Bastow, T. J. *J. Phys.-Condes. Matter* **1996**, *8*, 11309.

(73) Lipton, A. S.; Ellis, P. D. *J. Am. Chem. Soc.* **2007**, *129*, 9192.

(74) Lipton, A. S.; Heck, R. W.; Staeheli, G. R.; Valiev, M.; De Jong, W. A.; Ellis, P. D. *J. Am. Chem. Soc.* **2008**, *130*, 6224.

Table of Contents Artwork